Solid-State Light-Emitting Electrochemical Cells Based on Cationic Transition Metal Complexes for White Light Generation

Hai-Ching Su, Ken-Tsung Wong, and Chung-Chih Wu

Contents

Abstract Solid-state light-emitting electrochemical cells (LECs) based on cationic transition metal complexes (CTMCs) exhibit several advantages over conventional light-emitting diodes such as simple fabrication processes, low-voltage operation,

H.-C. Su (✉)
Institute of Lighting and Energy Photonics, National Chiao Tung University, No. 301, Gaofa 3rd Road, Guiren Township, Tainan County 711, Taiwan, ROC
e-mail: haichingsu@mail.nctu.edu.tw

K.-T. Wong
Department of Chemistry, National Taiwan University, No. 1, Sec. 4, Roosevelt Road, Taipei 106, Taiwan, ROC

C.-C. Wu (✉)
Department of Electrical Engineering, National Taiwan University, No. 1, Sec. 4, Roosevelt Road, Taipei 106, Taiwan, ROC
e-mail: chungwu@cc.ee.ntu.edu.tw

V.W.W. Yam (ed.), *WOLEDs and Organic Photovoltaics*, Green Energy and Technology,
DOI 10.1007/978-3-642-14935-1_4,

and high power efficiency. Hence, white CTMC-based LECs may be competitive for lighting applications. In this chapter, we review previous important works on CTMC-based LECs, such as increasing device efficiency, color tuning, lengthening device lifetime, and shortening turn-on time. Our demonstration of white CTMC-based LECs by using the host–guest strategy is then described.

1 Introduction

1.1 Features of Light-Emitting Electrochemical Cells

White organic light-emitting diodes (OLEDs) based on polymers and small-molecule materials have attracted much attention because of their potential applications in flat-panel displays and solid-state lighting [1–5]. Compared with conventional white OLEDs [6, 7], solid-state white light-emitting electrochemical cells (LECs) [8–10] possess several promising advantages. LECs generally require only a single emissive layer, which can be easily processed from solutions, and can conveniently use air-stable electrodes. The emissive layer of LECs contains mobile ions, which can drift toward electrodes under an applied bias. The spatially separated ions induce doping (oxidation and reduction) of the emissive materials near the electrodes, that is, p-type doping near the anode and n-type doping near the cathode [8–10]. The doped regions induce ohmic contacts with the electrodes and consequently facilitate the injection of both holes and electrons, which recombines at the junction between p- and n-type regions. As a result, a single-layered LEC device can be operated at very low voltages (close to E_g/e, where E_g is the energy gap of the emissive material and e is elementary charge) with balanced carrier injection, giving high power efficiencies. Furthermore, air-stable metals, for example, gold and silver, can be used since carrier injection in LECs is relatively insensitive to work functions of electrodes. Therefore, the power-efficient properties and easy fabrication processes make LECs competitive in solid-state lighting technologies.

In the past few years, cationic transition metal complexes (CTMCs) have also been increasingly studied for solid-state LECs because of the following several advantages over conventional LECs or polymer LECs (a) ion-conducting material is not needed since these metal complexes are intrinsically ionic and (b) higher electroluminescent (EL) efficiencies could be achieved due to the phosphorescent nature of the transition metal complexes. The development of solid-state LECs based on CTMCs thus will be described and discussed in this chapter.

1.2 Organization of This Chapter

This chapter is organized as follows. Section 2 reviews advances of LECs based on CTMCs, including topics of device efficiency (Sect. 2.1), colors (Sect. 2.2), device

lifetimes (Sect. 2.3), and turn-on times (Sect. 2.4). Section 3 is devoted to white LECs based on CTMCs. In Sect. 3.1, photophysical and electrochemical properties of newly developed blue-green and red emitting cationic iridium complexes are discussed. EL properties of white LECs based on host–guest cationic iridium complexes are then discussed in Sect. 3.2. Finally, we give an outlook about white LECs based on CTMCs.

2 Review of Light-Emitting Electrochemical Cells Based on Cationic Transition Metal Complexes

The first solid-state LEC was demonstrated with a polymer blend sandwiched between two electrodes [8]. The polymer blend was composed of an emissive conjugated polymer, a lithium salt (lithium trifluoromethanesulfonate), and an ion-conducting polymer (polyethylene oxide). The salt provides mobile ions and the ion-conducting polymer prevents this blend film from phase separation that may be induced by polarity discrepancy between the conjugated polymer and the salt. More recently, CTMCs have also been used in LECs, which show several advantages over conventional polymer LECs. In such devices, no ion-conducting material is needed since these metal complexes are intrinsically ionic. They generally show good thermal stability and charge-transport properties. Furthermore, high EL efficiencies are expected due to the phosphorescent nature of these metal complexes.

2.1 Increasing Device Efficiency

The first solid-state LEC based on transition metal complexes was reported in 1996 [11], where a ruthenium poly-pyridyl complex was utilized as the emissive material. Since then, many efforts have been made to improve performances of the LECs. In 1999, LECs based on low-molecular-weight ruthenium complexes were reported to have external quantum efficiency (EQE), which is defined as photons/electrons, of 1% [12]. In 2000, LECs using $[Ru(bpy)_3](ClO_4)_2$ (where bpy is 2,2′-bipyridine) with the gallium–indium eutectic electrode showed an EQE up to 1.8% [13]. Later, $[Ru(bpy)_3](PF_6)_2$ blended with poly(methyl methacrylate) (PMMA) was reported to improve the film quality and increase the EQE to 3% [14]. In 2002, a single-crystal LEC was made by repeatedly filling nearly saturated solution of $[Ru(bpy)_3](ClO_4)_2$ between two ITO (indium tin oxide) slides, followed by evaporating the solvent [15]. Such devices possessed low turn-on voltages and exhibited an EQE of 3.4%. Further improvement of performances was achieved by reducing self-quenching of excited states in $[Ru(bpy)_3]^{2+}$ with adding alkyl substituents on the bpy ligands [16], raising the EQE to 4.8% under the DC bias and to 5.5% under the pulsed driving. Yet a further improvement of the $[Ru(bpy)_3](ClO_4)_2$ device was

achieved by forming a heterostructure device, thus moving the emission zone away from the electrode and giving an efficiency of 6.4% [17].

More efficient cationic iridium complexes have also been used in LECs. In 2004, LECs based on the yellow-emitting (560 nm) cationic iridium complex $[Ir(ppy)_2(dtb\text{-}bpy)]PF_6$, where ppy is phenylpyridine and dtb-bpy is 4,4′-di-*tert*-butyl-2,2′-bipyridine, were reported, exhibiting efficiencies of 5% and 10 lm W^{-1} [18, 19]. On the one hand, replacing the ppy ligands by F-mppy ones, where F-mppy is 2-(4′-fluorophenyl)-5-methylpyridine, led to green emission (531 nm) and an EL efficiency of 1.8% [19, 20]. On the other hand, employing the $dF(CF_3)ppy$ ligands, where $dF(CF_3)ppy$ is 2-(2,4-difluorophenyl)-5-trifluoromethylpyridine, increased the energy gap of the cationic iridium complexes and shifted the EL emission to blue-green (500 nm, with an EQE of 0.75%) [21]. Another series of cationic phenylpyrazole-based iridium complexes were also recently reported to give blue (492 nm), green (542 nm), and red (635 nm) emission [22]. Blue, green, and red devices made of these complexes on poly(3,4-ethylenedioxythiophene):poly (styrene sulfonate) (PEDOT:PSS) coated ITO showed EQEs of 4.7%, 6.9%, and 7.4%, respectively.

Most LEC devices described above were made in a single-layered neat-film structure. In a neat film of an emissive material, interactions between closely packed molecules usually lead to quenching of excited states, detrimental to EQEs of devices. Thus, in addition to tuning of emission colors, the capability of the ligands to provide steric hindrance for suppressing self-quenching must also be carefully considered in designing ligands for emissive cationic metal complexes. In our previous studies of oligofluorenes, we had found that the introduction of aryl substitutions onto the tetrahedral C9 of oligofluorenes can provide effective hindrance to suppress interchromophore packing and self-quenching yet without perturbing energy gaps of the molecules [23–27], making the photoluminescent quantum yields (PLQYs) of oligo(9,9-diarylfluorene)s in neat films rather close to those in dilute solutions. Thus, we introduced 4,5-diaza-9,9′-spirobifluorene (SB) [28] as a steric and bulky auxiliary ligand of cationic iridium complexes, $[Ir(ppy)_2(SB)]PF_6$ (**1**) and $[Ir(dFppy)_2(SB)]PF_6$ (**2**) (Fig. 1), and investigate the influence of the SB ligand on reducing the self-quenching [29].

Spin-coated neat films of **1** and **2** exhibit PL spectra similar to those observed for their acetonitrile (MeCN) solutions (Fig. 2). However, spin-coated neat films of **1** and **2** show higher PLQYs (0.316 for **1**, 0.310 for **2**) and longer excited-state lifetimes (0.60 μs for **1**, 0.59 μs for **2**) than their MeCN solutions (Table 1). Since MeCN is a strongly polar solvent and the emitters are ionic, the photophysical properties of complexes **1** and **2** perhaps are significantly perturbed by strong solute–solvent interaction, rendering the observed PLQYs and lifetimes of **1** and **2** in MeCN less intrinsic. This indeed can be verified by measuring photophysical properties of **1** and **2** in a less polar solvent (yet still with enough solubility for spectroscopic measurements), such as dichloromethane (DCM). In DCM (5×10^{-5} M), both **1** and **2** exhibit longer excited-state lifetimes (0.79 μs for **1**, 0.42 μs for **2**) and higher PLQYs (0.467 for **1**, 0.364 for **2**) than in MeCN (Table 1).

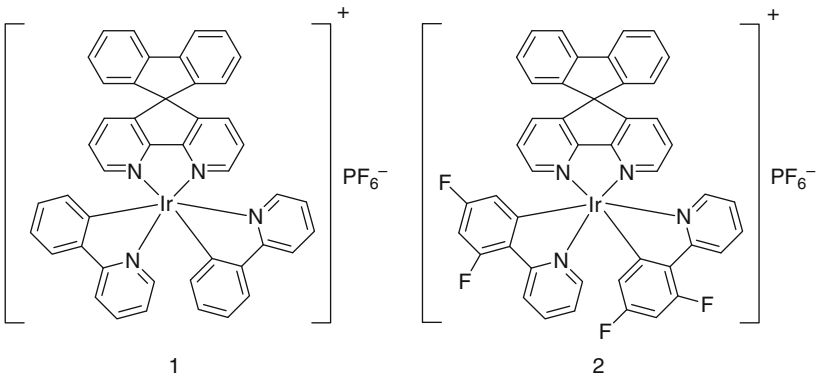

Fig. 1 Molecular structures of complexes **1** and **2**

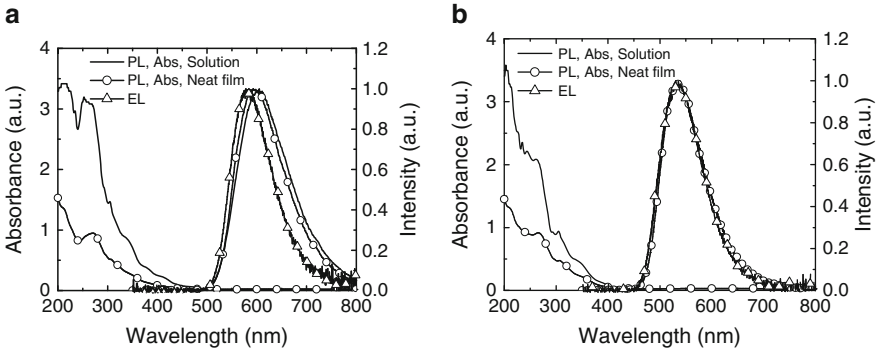

Fig. 2 Absorption and PL spectra in acetonitrile solutions and in neat films of (**a**) complex **1** and (**b**) complex **2**. Also shown in (**a**) and (**b**) are EL spectra of complex **1** and complex **2**, respectively. Reproduced with permission from [29]. Copyright 2007, WILEY-VCH Verlag GmbH & Co. KGaA, Weinheim

Thus, to better characterize the intrinsic photophysical properties of complexes **1** and **2** at the room temperature, complexes **1** and **2** were dispersed (with 1.5 mol%) in a large-gap thin-film host of *m*-bis(*N*-carbazolyl)benzene (mCP), which is rather nonpolar and has a large triplet energy. The measured PLQYs and excited-state lifetimes of the dispersed mCP films are (0.667, 0.81 μs) for **1** and (0.421, 0.74 μs) for **2** (Table 1). Thus **1** and **2** dilutely dispersed in mCP exhibit higher PLQYs and longer excited-state lifetimes than those in neat films. Shorter lifetimes in neat films indicate that interaction between closely packed molecules provides additional deactivation pathways, shortening excited-state lifetimes, and lowering the PLQYs. However, PLQYs of complexes **1** and **2** in neat films still retain ~50% and ~75% of those in mCP blend films. These are indeed rather high retaining percentages for PLQYs in neat films when compared with other phosphorescent molecules. For instance, [Ir(ppy)$_3$] [1.5 mol% dispersed in 4,4′-bis(carbazol-9-yl)

Table 1 Summary of physical properties of complexes **1** and **2**

Complex	$\lambda_{max,\ PL}$ (nm)[a]		PLQY, lifetime (μs)[b]		$E_{1/2}^{ox}$ (V)[c]	$E_{1/2}^{red}$ (V)[d]	$\Delta E_{1/2}$ (V)[e]
	Solution[f]	Neat film	Solution	Film			
1	605	593	0.226, 0.33[f] 0.467, 0.79[h] –, 4.31[j] –, 3.27[l]	0.316, 0.60[g] 0.667, 0.81[i] 0.381, 0.72[k]	1.35	−1.33	2.64
2	535	535	0.278, 0.39[f] 0.364, 0.42[h] –, 4.49[j] –, 4.29[l]	0.310, 0.59[g] 0.421, 0.74[i] 0.329, 0.55[k]	1.70	−1.26	2.92

[a]PL peak wavelength
[b]Photoluminescence quantum yields and the excited-state lifetimes
[c]Oxidation potential
[d]Reduction potential
[e]The electrochemical gap $\Delta E_{1/2}$ is the difference between $E_{1/2}^{ox}$ and $E_{1/2}^{red}$ corrected by potentials of the ferrocenium/ferrocene redox couple
[f]Measured in acetonitrile (5×10^{-5} M) at room temperature
[g]Neat films
[h]Measured in dichloromethane (5×10^{-5} M) at room temperature
[i]**1** and **2** were dispersed (1.5 mol%) in mCP films
[j]Measured in acetonitrile (5×10^{-5} M) at 77 K
[k]Films with 0.75 mol [BMIM][PF_6] per mole of **1** and **2**
[l]Measured in dichloromethane (5×10^{-5} M) at 77 K
Reproduced with permission from [29]. Copyright 2007, WILEY-VCH Verlag GmbH & Co. KGaA, Weinheim

biphenyl (CBP)] and bis[(4,6-difluorophenyl)pyridinato-*N*,C^2](picolinato)iridium (III) [FIrpic] (1.4 mol% dispersed in mCP) films had been reported to have very high PLQYs of 97 ± 2% and 99 ± 1%, respectively [30], while PLQYs of [Ir(ppy)$_3$)] and [FIrpic] neat films are only ~3% and ~15%, respectively. On the one hand, severe self-quenching in [Ir(ppy)$_3$] and [FIrpic] implies that the ppy, dFppy, and picolinic acid ligands cannot provide enough hindrance against intermolecular interactions in neat films. On the other hand, the high retaining percentages in neat-film PLQYs of complex **1** (with two ppy ligands and one SB ligand) and complex **2** (with two dFppy ligands and one SB ligand) compared with those in dispersed films indicate that SB ligands in these compounds provide effective steric hindrance and greatly reduce self-quenching. It is noted that self-quenching in neat films of [FIrpic] is not as severe as that in neat films of [Ir(ppy)$_3$]. It is likely that the fluoro substituents on the ppy ligands somewhat hinder the intermolecular interactions [30]. A similar effect is also observed here for complex **2**, which exhibits a higher PLQY retaining percentage (74%) than complex **1**.

In the operation of LEC devices, when a constant bias voltage is applied, a delayed EL response that is associated with the time needed for counterions in the LECs to redistribute under a bias is typically observed. For the cases of neat films of complexes **1** and **2**, the redistribution of the anions (PF_6^-) leads to the formation of a region of Ir(IV)/Ir(III) complexes (p-type) near the anode and a region of Ir(III)/Ir

(II) complexes (n-type) near the cathode [31]. With the formation of p- and n-regions near the electrodes, carrier injection is enhanced, leading to a gradually increasing device current and emission intensity. Devices based on neat films of complexes **1** and **2** (with the structure of glass substrate/ITO/complex **1** or **2** (100 nm)/Ag) exhibited very long response times. Very slow device response (e.g., tens of hours to reach the maximum brightness) had also been observed before for other LEC materials (e.g., $[Ru(bpy)_3](PF_6)_2$ derivatives with esterified ligands) [12]. Plausibly, bulky side groups on molecules impede the migration of ions. Thus to accelerate formation of the p- and n-doped regions in the emissive layer, 0.75 mol ionic liquid 1-butyl-3-methylimidazolium hexafluorophosphate $[BMIM][PF_6]$ per mole of complex **1** or **2** was added to provide additional anions (PF_6^-) [32].

It had been reported that in polymer LECs, incorporation of polar salts into conjugated polymer films might induce aggregates or phase separation due to discrepancy in polarity [33–35]. Thus, to study the effect of the $[BMIM][PF_6]$ addition on thin-film morphologies of complexes **1** and **2**, atomic force microscopy (AFM) of thin films was performed. As shown in Fig. 3, the AFM micrographs for films of complexes **1** and **2** with and without $[BMIM][PF_6]$ coated on ITO glass substrates show no significant differences and all give similar root-mean-square (RMS) roughness of ~1 nm. At this concentration of $[BMIM][PF_6]$ in complex **1** or **2** (0.75:1, molar ratio), no particular features of aggregation or phase separation were

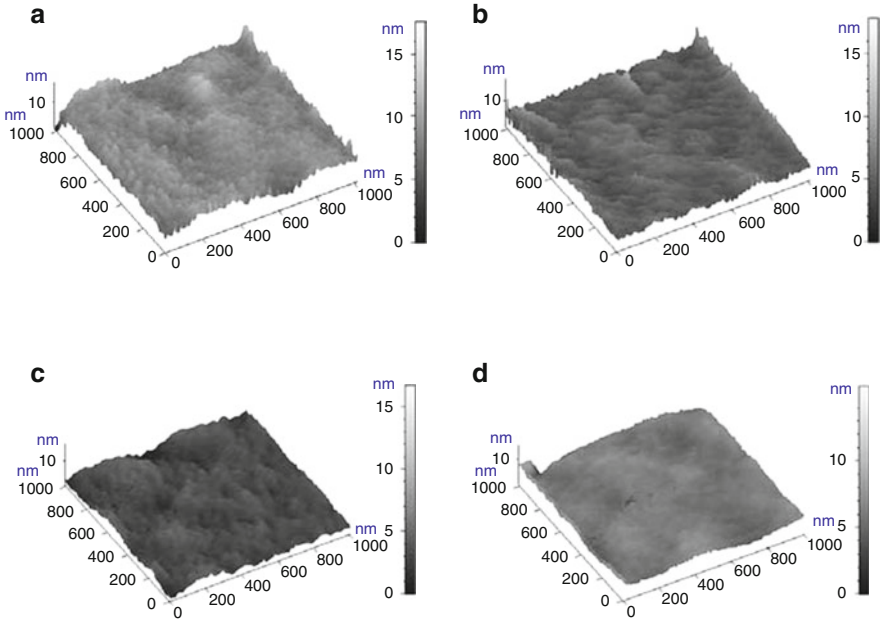

Fig. 3 3D AFM micrographs of (**a**) neat film of complex **1**, (**b**) blend film of $[BMIM][PF_6]$ and complex **1** (0.75:1, molar ratio), (**c**) neat film of complex **2**, and (**d**) blend film of $[BMIM][PF_6]$ and complex **2** (0.75:1, molar ratio). Reproduced with permission from [29]. Copyright 2007, WILEY-VCH Verlag GmbH & Co. KGaA, Weinheim

observed, and uniform spin-coated thin films could be routinely obtained. Such characteristics may be associated with the ionic nature of complexes **1** and **2**, which may make them more compatible with the added salts. Further, to examine the effects of the [BMIM][PF_6] addition on photophysical properties of complexes **1** and **2**, PLQYs and excited-state lifetimes of blend films were also measured and are shown in Table 1. In general, films of both **1** and **2** containing [BMIM][PF_6] (1:0.75, molar ratio) exhibit PLQYs and excited-state lifetimes comparable to those of neat films, indicating that the addition of [BMIM][PF_6] does not induce particular quenching of emission. Stable operation was also achieved in devices using such a formulation. In the following, device characteristics based on the structure of [glass substrate/ITO/**1**:[BMIM][PF_6] or **2**:[BMIM][PF_6] (100 nm)/Ag] are discussed and are summarized in Table 2.

A distinct characteristic of LECs is that they can be operated under a bias voltage close to E_g/e. As shown in Table 1, the electrochemical gaps ($\Delta E_{1/2}$), which were derived from the difference between $E^{ox}_{1/2}$ and $E^{red}_{1/2}$ corrected with potentials of the ferrocenium/ferrocene redox couple, for complexes **1** and **2** are 2.64 eV and 2.92 eV, respectively. The devices based on complexes **1** and **2** were thus first tested under the biases of 2.6 V and 2.9 V, respectively, although the energy gaps in films are usually smaller than those in solutions because of the environmental polarization. EL spectra of the devices based on complexes **1** and **2** (added with [BMIM][PF_6] are shown in Figs. 2a and 2b, respectively, for comparison with their PL spectra. EL spectra are basically similar to PL spectra, indicating similar emission mechanisms. Commission internationale de l'Eclairage (CIE) coordinates for the EL spectra of complexes **1** and **2** are (0.51, 0.48) and (0.35, 0.57), respectively. Time-dependent brightnesses and current densities of the devices operated under bias conditions described above are shown in Figs. 4a and 4b for complexes **1** and **2**, respectively. Both devices exhibited similar electrical characteristics. On the one hand, the currents of both devices first increased with time after the bias was applied and then stayed at a constant level after 350–400 min. On the other hand,

Table 2 Summary of the LEC device characteristics based on complexes **1** and **2**

Complex	Bias (V)	$\lambda_{max,\ EL}$ (nm)[a]	t_{max} (min)[b]	L_{max} cd m^{-2}	$\eta_{ext,\ max}$, $\eta_{p,\ max}$ (%, lm W^{-1})[d]	Lifetime (h)[e]
1	2.6	580	170	330	6.2, 19.0	26
	2.5		150	100	7.1, 22.6	54
2	2.9	535	85	145	6.6, 23.6	6.7
	2.8		90	52	7.1, 26.2	12

[a]EL peak wavelength
[b]Time required to reach the maximal brightness
[c]Maximal brightness achieved at a constant bias voltage
[d]Maximal external quantum efficiency and maximal power efficiency achieved at a constant bias voltage
[e]The time for the brightness of the device to decay from the maximum to half of the maximum under a constant bias voltage

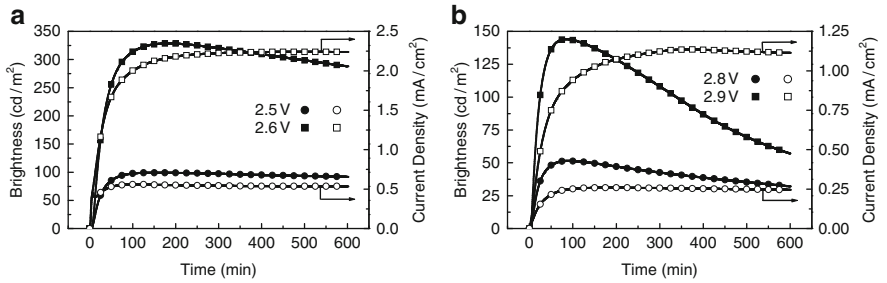

Fig. 4 The time-dependent brightness and current density of the single-layered LEC device for (**a**) complex **1** driven at 2.6 or 2.5 V and (**b**) complex **2** driven at 2.9 or 2.8 V. Reproduced with permission from [29]. Copyright 2007, WILEY-VCH Verlag GmbH & Co. KGaA, Weinheim

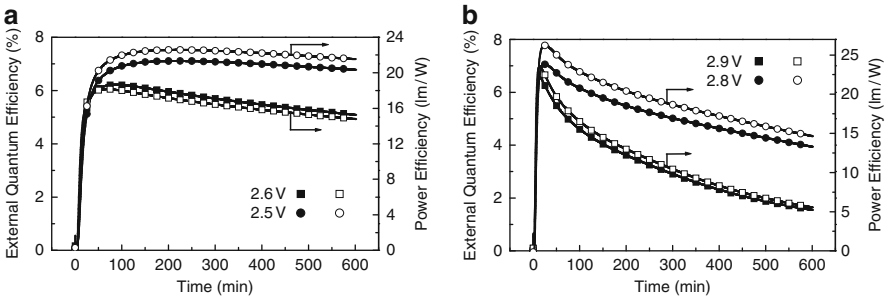

Fig. 5 The time-dependent EQE and the corresponding power efficiency of the single-layered LEC device for (**a**) complex **1** driven at 2.6 or 2.5 V and (**b**) complex **2** driven at 2.9 or 2.8 V. Reproduced with permission from [29]. Copyright 2007, WILEY-VCH Verlag GmbH & Co. KGaA, Weinheim

the brightness first increased with the current and reached the maximum of 330 cd m^{-2} for complex **1** at ~170 min and of 145 cd m^{-2} for complex **2** at ~85 min. The brightness then decreased with time even though the device current stayed rather constant. The decrease in brightness was irreversible, that is, the maximum brightness obtained in the first measurement could not be fully recovered in the followed measurements even under the same driving conditions. It is rationally associated with the degradation of the emissive material during the LEC operation, which was commonly seen in LEC devices [36].

Time-dependent EQEs and corresponding power efficiencies of the complex **1** device under the 2.6-V bias and the complex **2** device under the 2.9-V bias are shown in Figs. 5a and 5b, respectively. Both devices exhibited similar time evolution in EQE. When a forward bias was just applied, the EQE was rather low due to unbalanced carrier injection. During the formation of the p- and n-type regions near electrodes, the balance of the carrier injection was improved and the EQE of the device thus increased rapidly. The peak EQE and the peak power efficiency are

(6.2%, 19.0 lm W^{-1}) for the complex **1** device under the 2.6-V bias and (6.6%, 23.6 lm W^{-1}) for the complex **2** device under the 2.9-V bias. One notices that the peak efficiencies occurred before the currents reached their final maximal values. Such a phenomenon may be associated with two factors. First, although with the formation of the p- and n-type regions near electrodes, both contacts are becoming more ohmic and the carrier injection at both electrodes are becoming more balanced; however, the carrier recombination zone may consequently move toward one of the electrodes because of discrepancy in electron and hole mobilities. The recombination zone moving to the vicinity of an electrode may cause exciton quenching such that the EQE of the device would decrease with time while the current and the brightness are still increasing. Besides, degradation of the emissive material under a high field would also contribute to the decrease in the EQE when the recombination zone is still moving or when the recombination zone is fixed.

Both LEC devices driven under 0.1-V lower biases exhibit higher peak EQEs and lower degradation rates. As shown in Figs. 5a and 5b, the peak EQE and the peak power efficiency are (7.1%, 22.6 lm W^{-1}) for the complex **1** device under the 2.5-V bias and (7.1%, 26.2 lm W^{-1}) for the complex **2** device under the 2.8-V bias. It is interesting to note that the peak EQEs of the single-layered devices (no PEDOT:PSS is used) based on complexes **1** and **2** approximately approach the upper limits that one would expect from the PLQYs of their neat films, when considering an optical out-coupling efficiency of ~20% from a typical layered light-emitting device structure. To our knowledge, these EQEs are among the highest values reported for orange-red (or yellow) and green solid-state LECs based on CTMCs. Such results indicate that CTMCs with superior steric hindrance are essential and useful for achieving highly efficient solid-state LECs.

Since these newly developed cationic complexes (**1** and **2**) are intrinsically efficient, to further reduce self-quenching and increase EL efficiency, one possible approach is to spatially disperse the emitting complex (guest) into a matrix complex (host), as previously reported for conventional OLEDs and solid-state LECs [37–39]. The mixed host–guest films (~100 nm) for PL studies were spin-coated onto quartz substrates using mixed solutions of various ratios. Since in LECs, a salt [BMIM][PF_6] of 19 wt% (where BMIM is 1-butyl-3-methylimidazolium) was also added to provide additional mobile ions and to shorten the device response time [29, 32], PL properties of the host–guest–salt three-component system were also characterized.

Figure 6a shows the absorption spectrum of the guest and the PL spectra of the host–guest two-component systems having various guest concentrations. With the increase of the guest concentration, a gradual red shift from the host-like emission to the guest-like emission is observed. As shown in Fig. 6b, the highest PLQY of ~37% (vs. ~31% of neat host and guest films) is obtained at the guest concentration of 25 wt%, at which the emission is nearly completely from the guest. Accompanying this enhanced PLQY is the longer excited-state lifetime (0.69 μs) when compared with those of neat films (0.59 μs for the host and 0.60 μs for the guest), indicating the effectiveness of the dispersion in suppressing quenching mechanisms of guest molecules. Less complete transfer is observed at lower guest concentrations,

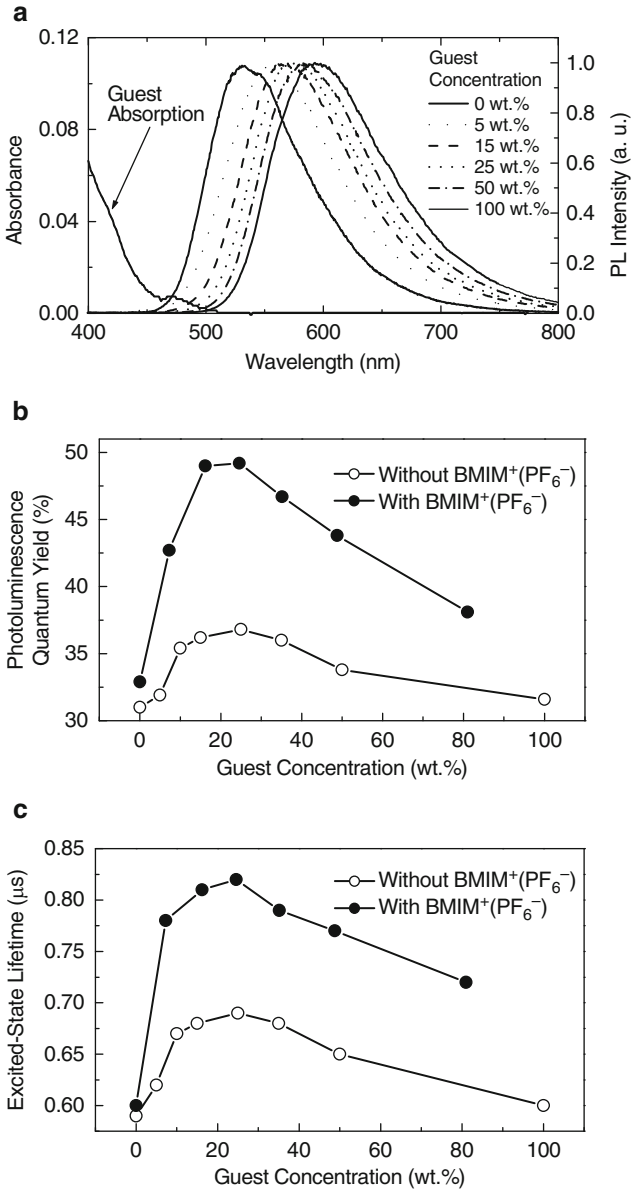

Fig. 6 (**a**) The absorption spectrum of the neat guest film and PL spectra of host–guest films with various guest concentrations (without [BMIM][PF_6]. (**b**) Photoluminescence quantum yields and (**c**) excited-state lifetimes as a function of the guest concentration for host–guest films without and with [BMIM][PF_6] (19 wt%). Reproduced with permission from [49]. Copyright 2006, American Institute of Physics

which may be associated with the less extensive overlap between the host emission and the weak guest absorption. A calculation of the Förster radius for the host–guest energy transfer gives a small value of <16 Å [40] indicating inefficient energy transfer at lower guest concentrations. With the addition of [BMIM][PF_6] (19 wt%), the trend in PL properties [spectra (not shown), PLQYs (Fig. 6b), and lifetimes (Fig. 6c)] as a function of the guest concentration is similar to those of the two-component system. Yet, an even higher PLQY of ~50% (about 1.6× enhancement compared with PLQYs of neat host and guest films) and longer excited-state lifetime of ~0.82 μs are observed around the guest concentration of 25 wt%. It appears that [BMIM][PF_6] not only provides additional mobile ions but is also effective in suppressing interchromophore quenching.

Figure 7a shows the time-dependent brightness and current density under constant biases of 2.5–2.7 V for the LEC using the mixture giving the highest PLQY (i.e., with host, guest, and [BMIM][PF_6] concentrations of 56 wt%, 25 wt%, and 19 wt%, respectively). After the bias was applied, on the one hand, the current first increased and then stayed rather constant. On the other hand, the brightness first increased with the current and reached the maxima of 10, 30, and 75 cd m^{-2} at <1 h under biases of 2.5 V, 2.6 V, and 2.7 V, respectively. The brightness then dropped with time with a rate significantly depending on the bias voltage (or current). Corresponding time-dependent EQEs and power efficiencies of the same device are shown in Fig. 7b. When a forward bias was just applied, the EQE was rather low due to poor carrier injection. During the formation of the p- and n-type regions near electrodes, the capability of carrier injection was improved and the EQE thus rose rapidly. The peak EQE, current, and peak power efficiencies at 2.5 V, 2.6 V, and 2.7 V are (10.4%, 29.3 cd A^{-1}, 36.8 lm W^{-1}), (9.9%, 27.9 cd A^{-1}, 33.7 lm W^{-1}), and (9.4%, 26.5 cd A^{-1}, 30.8 lm W^{-1}), respectively.

The maximum current density vs. voltage characteristics of LECs with various guest concentrations are shown in Fig. 8a. The bias voltage required for same

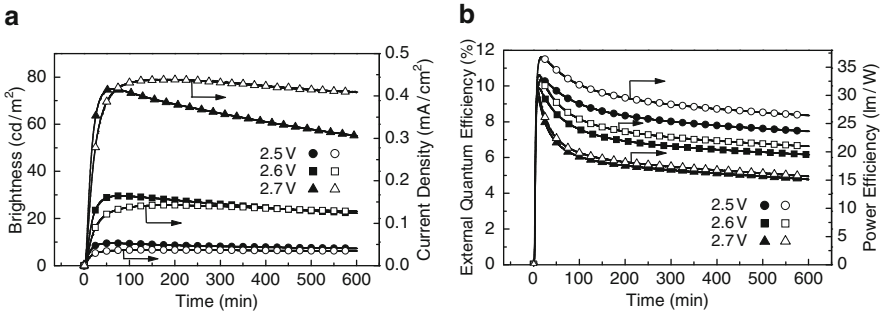

Fig. 7 (**a**) Brightness (*solid symbols*) and current density (*open symbols*) and (**b**) external quantum efficiency (*solid symbols*) and power efficiency (*open symbols*) as a function of time under a constant bias voltage of 2.5–2.7 V for the host–guest LEC with host, guest and [BMIM][PF_6] concentrations of 56 wt%, 25 wt%, and 19 wt%, respectively. Reproduced with permission from [49]. Copyright 2006, American Institute of Physics

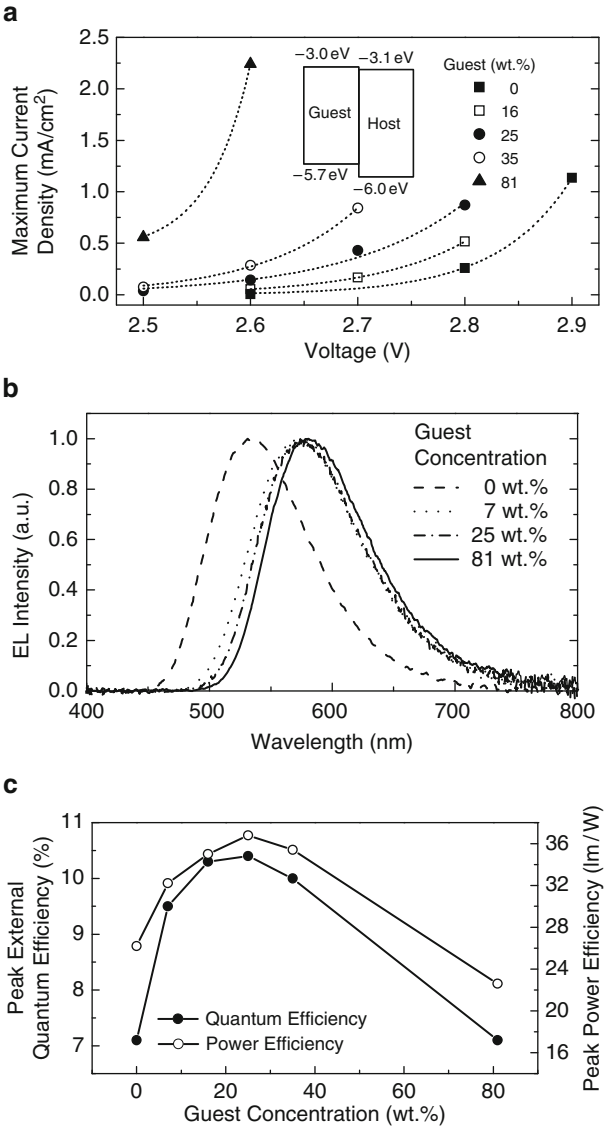

Fig. 8 (**a**) Maximum current density vs. voltage characteristics for LECs with various guest concentrations. (**b**) EL spectra (at 2.8 V) for LECs with various guest concentrations. (**c**) Peak external quantum efficiencies and peak power efficiencies (at current densities <0.1 mA cm^{-2}) of host–guest LECs as a function of the guest concentration. *Inset* of (**a**): the energy level diagram of the host and guest molecules. Reproduced with permission from [49]. Copyright 2006, American Institute of Physics

current drops as the guest concentration is raised. This may be understood by the energy level diagram obtained from cyclic voltammetry [29] (inset of Fig. 8a). Such an energy level alignment favors carrier injection/transport (at least for holes) through the smaller-gap guest and direct carrier recombination/exciton formation on the guest (rather than host–guest energy transfer) if the guest concentration is high enough. EL spectra of host–guest LECs with various guest concentrations (Fig. 8b) indeed support the mechanism of direct exciton formation on guest molecules, which would greatly reduce host emission due to incomplete energy transfer. Compared with PL spectra (e.g., Fig. 6), EL spectra are much less dependent on the guest concentration. Even with a guest concentration as low as 7 wt%, the EL spectrum is almost the same as that of the pure guest device [i.e., the LEC with 81 wt% of guest and 19 wt% of [BMIM][PF_6], indicating predominant guest emission.

Figure 8c shows peak EQEs and peak power efficiencies for host–guest LECs as a function of the guest concentration (at current densities <0.1 mA cm^{-2}). The peak EQEs and power efficiencies roughly follow the trend of the PLQYs. The highest peak EQE and power efficiency of 10.4% and 36.8 lm W^{-1} are achieved at the guest concentration of 25 wt%, coincident with the concentration giving the highest PL efficiency. Such an EQE represents a 1.5× enhancement compared with those of pure host and guest devices. It is also worth noting that such a peak EQE approximately approaches the upper limit that one would expect from the PLQY of the host–guest emissive layer (~50%), when considering an optical out-coupling efficiency of ~20% from a typical layered light-emitting device structure. Such EQEs and power efficiencies also are among the highest reported for solid-state LECs based on CTMCs. Such results indicate that the host–guest system is essential and useful for achieving highly efficient solid-state LECs.

2.2 *Color Tuning*

Early developments of CTMCs for LECs were focused on ruthenium-based complexes, which typically emit in the red and orange–red part of the spectrum due to low metal-to-ligand charge transfer (MLCT) energies. Ester-substituted ligands have been found to red-shift the emission of [$Ru(bpy)_3$](PF_6)$_2$ [12, 13]. Ng et al. [41] published a series of polyimides containing a Ru complex on the main chain. The device showed deep-red EL centered at about 650 nm and near infrared (IR) emission centered near 750–800 nm. However, the efficiency of such device is rather low (0.1%). Bolink et al. [42] also have achieved a deep red emission, using bis-chelated Ru complex [Ru(tpy)(tpy-CO_2Et)](PF6)$_2$, where tpy is terpyridine. The ester substituents were found to significantly improve the device efficiency over the unsubstituted terpyridyl complex, but the device efficiency is still very low. Low efficiency is a general phenomenon of terpyridyl Ru complexes since the luminescent ^{3}MLCT state is quenched by low-lying ^{3}MC levels due to poor bite angles of the tpy ligands [43].

Iridium was shown to have promise for color tuning over ruthenium complexes because of increased ligand-field splitting energies. The pioneering work of Ir-based complex ($[Ir(ppy)_2(dtb\text{-}bpy)]PF_6$ for LECs was reported by Slinker et al. [18]. Subsequent color tuning of CTMCs has centered on appropriate selection of ligand or transition metal core. Complexes based on fluorine substituents on the phenylpyridine ligands were reported to cause a blue shift of the emission spectrum relative to unfluorinated complexes. For example, ($[Ir(ppy)_2(dtb\text{-}bpy)]PF_6$ and $[Ir(dF(CF_3)ppy)_2(dtb\text{-}bpy)]PF_6$ showed EL centered at 542 nm and 500 nm, respectively [20, 21]. The increasing of bandgap of complexes results from the fact that metal-centered highest occupied molecular orbital (HOMO) level is highly stabilized by introduction of the fluorine atoms [21]. We also studied the electrochemical characteristics of complexes **1** and **2** via cyclic voltammetry. As shown in Fig. 9, complex **2** exhibits a reversible oxidation peak at 1.70 V vs. Ag/AgCl, which is significantly higher than that of complex **1** (1.35 V). The HOMO level of ($[Ir(ppy)_2(dtb\text{-}bpy)]PF_6$ had been reported to be a mixture of the d-orbitals of iridium and the π-orbitals of the phenyl ring of the ppy ligand [21]. Since **1** and **2** are also cationic ppy-based Ir(III) complexes, their HOMO distributions should be similar to that of ($[Ir(ppy)_2(dtb\text{-}bpy)]PF_6$. The higher oxidation potential of complex **2** compared with that of complex **1** indicates that the two electron-withdrawing fluoro substituents on the phenyl ring of the ppy ligand possibly reduce the electron density on the Ir metal center and consequently stabilize the HOMO level. According to the previous studies, the lowest unoccupied molecular orbital (LUMO) of ($[Ir(ppy)_2(dtb\text{-}bpy)]PF_6$ is located mainly on the dtb-bpy ligand [21], and therefore, for complexes **1** and **2**, reduction is expected to take place on the auxiliary SB ligand. Similar reduction potentials for complex **1** (–1.33 V) and complex **2** (–1.26 V) confirm that this common ligand is responsible for reduction of both compounds. Still, the reduction potential of complex **2** is slightly less negative than

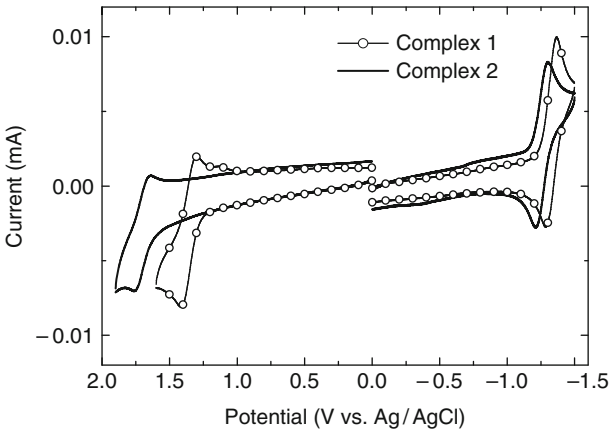

Fig. 9 Cyclic voltammograms of complexes **1** and **2**. Potentials were recorded vs. the reference electrode Ag/AgCl (sat'd). Reproduced with permission from [29]. Copyright 2007, WILEY-VCH Verlag GmbH & Co. KGaA, Weinheim

that of complex **1** perhaps because the fluoro substituents make complex **2** more electrophilic and thus easier to reduce [21]. With the HOMO level being significantly shifted and the LUMO level being only slightly changed by fluoro substitution, the PL emission of complex **2** is significantly blue shifted compared with PL of complex **1**, reflecting a characteristic of Ir complexes that their energy gaps can be tuned through introducing substituents of different electronic properties on the ppy ligands.

Tamayo et al. [22] demonstrated tuning of the emission color across a large portion of the visible part of the spectra by independent tuning of the HOMO and LUMO levels of the parent complex $[Ir(ppy)_2(bpy)]PF_6$, where ppz is 1-phenylpyrazolyl. Highly efficient red ($\lambda_{max} = 635$ nm), green ($\lambda_{max} = 542$ nm), and blue ($\lambda_{max} = 492$ nm) EL emissions were obtained in LECs based on $[Ir(tbppz)_2(biq)]PF_6$, $[Ir(ppy)_2(bpy)]PF_6$, and $[Ir(dF\text{-}ppz)_2(dtb\text{-}bpy)](PF_6)$, where tb is 5′-*tert*-butyl and biq is 2,2′-biquinoline [22].

Color tuning can also be achieved by destabilization of the LUMO rather than stabilization of the HOMO. Nazeeruddin et al. [44] achieved blue-green EL emission ($\lambda_{max} = 520$ nm) in LECs based on $[Ir(ppy)_2(dma\text{-}bpy)]PF_6$, where dma-bpy is 4,4′-(dimethylamino)-2,2′-bipyridine. Introduction of the electron-donating dimethylamino groups was demonstrated to significantly destabilize the LUMO relative to the HOMO when compared with the parent complex $[Ir(ppy)_2(dtb\text{-}bpy)]PF_6$, resulting in blue-shifted emission.

Attaching a charged side group on the periphery of the cyclometalating ligands proposed by Bolink et al. [45] converted a neutral complex into a CTMC. A blue-green emission ($\lambda_{max} = 487$ nm) was observed for $[Ir(ppy\text{-}PBu_3)3](PF_6)_3$. Such a blue shift in emission, compared with the $[Ir(ppy)_3]$ complex, was attributed to the electron-withdrawing nature of the tri-butylphosphonium group on the phenylpyridine ligand. However, EL was found to change from blue-green to yellow ($\lambda_{max} = 570$ nm) after 100 s of operation at 4 V.

Recently, we have also developed a novel blue-green emitting ppz-based Ir-complex (stable EL $\lambda_{max} = 488$ nm) and a saturated red emitting ppy-based Ir-complex (PL $\lambda_{max} = 672$ nm). Details of photophysical and EL properties of these two complexes will be described in Sect. 3.

2.3 Lengthening Device Lifetime

The lifetimes of the devices defined as the time it takes for the brightness of the device to decay from the maximum to half of the maximum under a constant bias are important figure-of-merit when evaluating the durability of devices for display or lighting applications. Much effort has been made to lengthen device lifetimes of LECs.

The rates of electrochemical reactions of emissive CTMCs under electrical driving are bias dependent. In general, running LEC devices at a higher luminance

leads to shorter lifetimes, so long lifetime can often be claimed at the expense of luminance [12, 29, 46–49]. The lifetimes for complex **1** under the 2.6-V driving and for complex **2** under the 2.9-V driving are ~26 h (extrapolated) and 6.7 h, respectively (Fig. 4). Although operated under a lower current density, the lifetime of the complex **2** device is significantly shorter than that of the complex **1** device. Irreversible multiple oxidation and subsequent decomposition under a high electric field had been proposed as the mechanism for degradation of LECs based on cationic iridium complexes [32, 50]. Since a higher bias voltage is required for operating the device based on complex **2** due to its larger energy gap, the higher electric field in the emissive layer of the complex **2** device perhaps accelerated the degradation. To mitigate the device degradation, slightly lower bias voltages of 2.5 V and 2.8 V were then applied for testing the devices based on complex **1** and complex **2**, respectively. As shown in Figs. 4a and 4b, slight reduction of the applied bias by 0.1 V had led to greatly reduced degradation rates for brightnesses of both devices. The lifetimes of the complex **1** device under the 2.5-V driving and the complex **2** device under the 2.8-V driving are ~54 and ~12 h (both extrapolated), roughly two times longer than those driven at 0.1-V higher bias voltages. The longer device lifetimes, however, are achieved at the expense of reduced brightness. Therefore, emissive materials with high quantum yields are essential for LECs to be operated at a practical brightness yet using a lowest possible bias, which would ensure long-lifetime operation of LECs.

Blending CTMCs in an inert polymer can also improve lifetime [14, 16]. It may result from lowered current density caused by separation of conducting chromophores in LEC devices. The choice of metal contacts was found to influence the lifetime, even for devices stored in the off state because reactive metal (e.g., Al) may activate some electrochemical reactions with CTMCs and lead to degradation [14, 51]. Degradation of $[Ru(bpy)_3]^{2+}$-based device involves the water-induced formation of photoluminescence quenchers, which were suggested to be complexes such as $[Ru(bpy)_2(H_2O)_2]^{2+}$ and $[Ru(bpy)_2(H_2O)]_2O^{4+}$ [36, 52, 53]. Thus, CTMCs with phenanthroline ligands credited with improved hydrophobicity increased resistance toward water-induced substitution reactions, leading to the higher device stability. $[Ir(ppy)_2(dp\text{-}phen)]PF_6$ device, where dp-phen is 4,7-diphenyl-1,10-phenanthroline, was found by Bolink et al. to have a lifetime of 65 h, which is the highest reported for a neat-film Ir-based LEC to date [54].

2.4 Shortening Turn-On Time

Turn-on time is defined as the time required for LEC devices to reach maximum emission under dc bias. For practical applications, turn-on times must be significantly reduced; however, most schemes for improving turn-on time come at a cost to stability.

Higher applied biases can lead to faster turn-on, but results in shorter lifetimes [12, 48]. To achieve faster turn-on without losing the stability, a pulsed-biasing

scheme – a short pulse at a higher voltage was used to turn the device on, followed by a lower voltage that was used to drive the device for extended periods, was proposed by Handy et al. [12]. However, such technique complicates the driving circuits and the integration for applications. Reducing the thickness of the emissive layer of LECs also can reduce the turn-on time, but leads to a decrease in the device efficiency due to exciton quenching near the electrodes [55]. Smaller counterions such as BF_4^- or ClO_4^- lead to faster turn-on times than larger one, e.g., PF_6^-, but also deteriorate device lifetimes [13, 16]. Increasing ionic conductivity of the emissive layer by addition of an electrolyte to the CTMC layer has been shown to improve device lifetimes due to additional ions [20, 32, 56, 57]. However, device lifetimes were deteriorated as well.

Chemically attaching ionically charged ligands to metal complexes represents an alternative and promising approach to increase the ionic conductivity and to improve the turn-on speed of LECs, since the phase compatibility is less an issue in such configurations. Bolink et al. reported a homoleptic iridium complex containing ionically charged ligands, giving a net charge of +3 for each complex [45]. The LEC based on such complex showed a much improved turn-on time, yet also suffered other issues, e.g., color shift during operation and low efficiencies, which are relevant to practical applications as well. Zysmen-Colman et al. recently also reported homoleptic ruthenium-based and heteroleptic iridium-based CTMCs containing tethered ionic tetraalkylammonium salts [58]. Similarly, LECs constructed using such complexes also exhibited reduced turn-on times; yet EL efficiencies from these complexes are not satisfactory, compared with general EL efficiencies achievable with CTMCs. Hence, further studies on CTMCs containing ionically charged ligands that can give improved turn-on times, stable operation, and also high device efficiency are still highly desired.

In one of our previous works, we demonstrated the reduction in turn-on times of single-component Ir-based LECs with tethered imidazolium moieties. The new CTMC is achieved by fusing two imidazolium groups at the ends of the two alkyl side chains of a more conventional complex $[Ir(ppy)_2(dC6\text{-}daf)]PF_6$ (**3**) (where dC6-daf is 9,9′-dihexyl-4,5-diazafluorene), forming the new complex $[Ir(ppy)_2(dCMIM\text{-}daf)](PF_6)_3$ (**4**) (where dC6MIM-daf is 9,9-bis[6-(3-methylimidazolium)hexyl]-1-yl-4,5-diazafluorene) [59]. Molecular structures of complexes **3** and **4** are shown in Fig. 10.

Homogeneous thin films of both complexes **3** and **4** can be obtained by spin-casting from CH_3CN solution. We also tried to prepare a physical blending film of **3** and ionic liquid [BMIM][PF_6] for comparative studies; however, the resulting cloudy films indicated strong phase separation and incompatibility between complex **3** with the long alkyl chains and the ionic liquid with high polar character. The UV-visible absorption and PL spectra of **3** and **4** in CH_2Cl_2 solution (10^{-5} M) and in neat film (~100 nm) are shown in Figs. 11a and 11b, respectively. Similar absorption features are observed in either solutions or films for both complexes. Solution PL emission is in the yellow range (~570 nm) for both complexes **3** and **4**, indicating tethering imidazolium groups at the ends of the alkyl chains in complex **3** has no significant effects on modulating energy gaps.

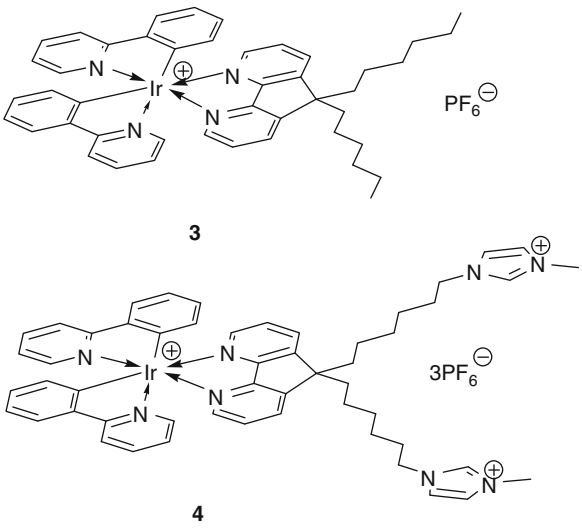

Fig. 10 Molecular structures of complexes **3** and **4**

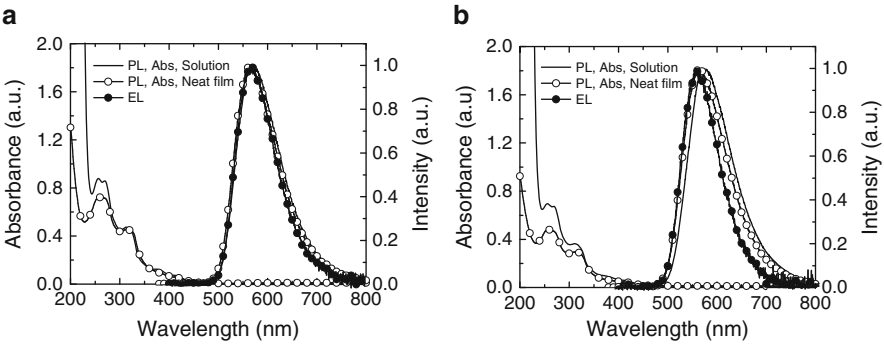

Fig. 11 Absorption and PL spectra in CH_2Cl_2 solution (10^{-5} M) and in neat film along with EL spectra under a forward bias voltage of 2.8 V for (**a**) complex **3** and (**b**) complex **4**, respectively. Reproduced with permission from [59]. Copyright 2008, WILEY-VCH Verlag GmbH & Co. KGaA, Weinheim

The PLQYs of complexes **3** and **4** in CH_2Cl_2, as determined with a calibrated integrating sphere, are 0.59 and 0.47, respectively (Table 3). Room-temperature transient PL of complexes **3** and **4** in CH_2Cl_2, as determined by the time-correlated single photon counting technique, exhibits the single-exponential decay behavior, and the extracted excited-state lifetimes for **3** and **4** are 1.12 μs and 0.94 μs, respectively (Table 3). Spin-coated neat films of complexes **3** and **4** exhibit PL spectra similar to those observed for their solutions (Fig. 11). The measured PLQYs and excited-state lifetimes of the neat films are (0.33, 0.66 μs) for **3** and (0.35, 0.75 μs) for **4** (Table 3). Lower PLQYs and shorter excited-state lifetimes in neat

Table 3 Summary of physical properties of complexes **3** and **4**

Complex	$\lambda_{max,\ PL}$ (nm)[a]		PLQY[b]		τ (μs)[c]		$E^{ox}_{1/2}$ (V)[d]	$E^{red}_{1/2}$ (V)[e]	$\Delta E_{1/2}$ (V)[f]
	Solution[g]	Neat film	Solution[g]	Neat film	Solution[g]	Neat film			
3	568	562	0.59	0.33	1.12	0.66	+1.33	−1.47	2.80
4	570	562	0.47	0.35	0.94	0.75	+1.31	−1.48	2.82

[a]PL peak wavelength
[b]Photoluminescence quantum yields
[c]Excited-state lifetimes
[d]Oxidation potential
[e]Reduction potential
[f]The electrochemical gap $\Delta E_{1/2}$ is the difference between $E^{ox}_{1/2}$ and $E^{red}_{1/2}$
[g]Measured in CH_2Cl_2 (10^{-5} M) at room temperature
Reproduced with permission from [59]. Copyright 2008, WILEY-VCH Verlag GmbH & Co. KGaA, Weinheim

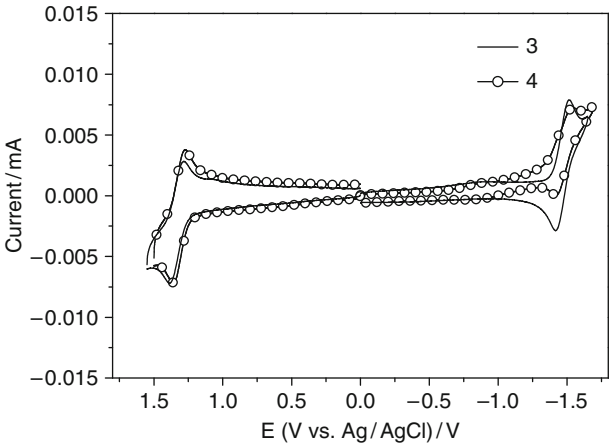

Fig. 12 Cyclic voltammogram of complexes **3** and **4**. All potentials were recorded vs. Ag/AgCl (sat'd) as a reference electrode. Reproduced with permission from [59]. Copyright 2008, WILEY-VCH Verlag GmbH & Co. KGaA, Weinheim

films indicate that interaction between closely packed molecules provides additional deactivation pathways. However, PLQYs of complexes **3** and **4** in neat films still retain ~56% and ~75% of those in solutions. Highly retained PLQYs in neat films of complexes **3** and **4** are likely to be associated with their sterically bulky dC6-daf and dC6MIM-daf ligands. It is noted that self-quenching in neat films of complex **4** is not as severe as that in neat films of complex **3** perhaps due to better steric hindrance provided by imidazolium groups in complex **4**.

Figure 12 depicts the electrochemical characteristics of complexes **3** and **4** probed by cyclic voltammetry and the measured redox potentials are summarized in Table 3. Complexes **3** and **4** exhibit reversible redox peaks at similar potential

(vs. Ag/AgCl); one reversible oxidation potential occurs at 1.33 V and 1.31 V for **3** and **4**, respectively, while one reversible reduction potential occurs at –1.47 V and –1.48 V for **3** and **4**, respectively. The HOMO of $[Ir(ppy)_2(N^N)]PF_6$ complexes has been reported to be a mixture of the iridium and the phenyl group of the C^N ligand, while the LUMO mostly localizes on the N^N ligand [21]. Since the structures of complexes **3** and **4** differ only in the terminal alkyl chain of N^N ligand, their HOMO and LUMO distribution should be similar and give similar redox potentials. The presence of imidazolium moieties in **4** exhibited limited influence on the electrochemical properties of the Ir-center, especially the frontier molecular orbitals.

Device characteristics based on the structure of [glass substrate/ITO/complex **3** or **4** (100 nm)/Ag] are discussed and are summarized in Table 4. EL spectra of the devices based on complexes **3** and **4** are shown in Figs. 11a and 11b, respectively, for comparison with their PL spectra. EL spectra are basically similar to PL spectra, indicating similar emission mechanisms. Time-dependent brightness and current densities of the LEC devices based on complex **3** operated under 2.7 and 2.8 V are shown in Fig. 13a. The currents of devices increased slowly with time after the bias was applied and kept increasing even after 10-h operation. The turn-on time of the device ($t_{turn\text{-}on}$), defined as the time to achieve brightness of 1 cd cm^{-2}, was 65 min under 2.8 V. The brightness increased with the current and reached the maximum of 105 cd m^{-2} at ~500 min under 2.8 V. For devices under 2.7 V, the brightness reached 56 cd m^{-2} and was still increasing at 600 min. Comparatively, the LECs based on complex **4** showed much faster response. As shown in Fig. 13b, this device turned on sharply in 12 min under 2.8 V, it took only ~200 min for the devices to reach the maximal brightness of 79 cd m^{-2} and 31 cd m^{-2} under 2.8 V and 2.7 V, respectively. Such improved turn-on times confirm that the chemically tethering imidazolium groups onto complex **4** increase the density of mobile counterions (PF_6^-) in neat films and consequently increase the neat-film ionic conductivity.

Table 4 Summary of the LEC device characteristics based on complexes **3** and **4**

Complex	Bias (V)	$\lambda_{max,\ EL}$ (nm)[a]	$t_{turn\text{-}on}$ (min)[b]	t_{max} (min)[c]	L_{max} (cd m^{-2})[d]	$\eta_{ext,\ max}$, $\eta_{p,\ max}$ (%, lm W^{-1})[e]
3	2.8	566	65	500	105	5.5, 18.7
	2.7		84	>600	>56[f]	5.5, 19.2
4	2.8	577	12	200	79	4.0, 14.7
	2.7		16	200	31	4.5, 17.1

[a]EL peak wavelength
[b]Time required reaching the brightness of 1 cd cm^{-2}
[c]Time required to reach the maximal brightness
[d]Maximal brightness achieved at a constant bias voltage
[e]Maximal external quantum efficiency and maximal power efficiency achieved at a constant bias voltage
[f]Maximal brightness was not reached during a 10-h measurement
Reproduced with permission from [59]. Copyright 2008, WILEY-VCH Verlag GmbH & Co. KGaA, Weinheim

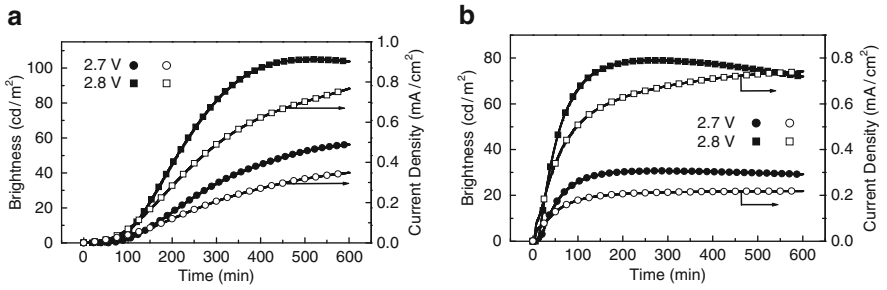

Fig. 13 Time-dependent brightness and current density under 2.7 V and 2.8 V for the single-layered LEC device based on (**a**) complex **3** and (**b**) complex **4**, respectively. Reproduced with permission from [59]. Copyright 2008, WILEY-VCH Verlag GmbH & Co. KGaA, Weinheim

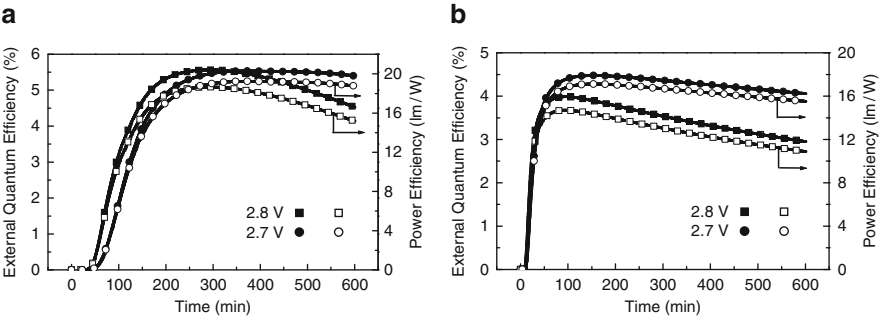

Fig. 14 Time-dependent EQE and the corresponding power efficiency under 2.7 V and 2.8 V for the single-layered LEC device based on (**a**) complex **3** and (**b**) complex **4**, respectively. Reproduced with permission from [59]. Copyright 2008, WILEY-VCH Verlag GmbH & Co. KGaA, Weinheim

Efficient LECs are essential for operation at a practical brightness yet using a lowest possible bias, which would ensure stable operation of LECs. Hence, it is important to examine the effect of chemical tethering of imidazolium groups with an ionic iridium complex on the device efficiencies of LECs. Time-dependent EQEs and corresponding power efficiencies of the complex **3** and **4** devices under biases of 2.7 V and 2.8 V are shown in Figs. 14a and 14b, respectively. When a forward bias was just applied, the EQE was rather low due to unbalanced carrier injection. During the formation of the p- and n-type regions near electrodes, the balance of the carrier injection was improved and the EQE of the device thus increased rapidly. The peak EQE and the peak power efficiency are (5.5%, 18.7 lm W^{-1}) and (5.5%, 19.2 lm W^{-1}) for the complex **3** device under biases of 2.8 V and 2.7 V, respectively. The time-dependent evolution trend in device efficiency of the complex **4** device is similar to that of the complex **3** device, yet it took much less time (within 100 min) for the complex **4** device to reach the peak device efficiency. The peak EQE and the peak power efficiency are (4.0%,

14.7 lm W^{-1}) and (4.5%, 17.1 lm W^{-1}) for the complex **4** device under 2.8 V and 2.7 V, respectively. EL efficiencies of devices based on both complexes **3** and **4** are comparable, indicating chemical tethering of imidazolium groups with an ionic iridium complex benefits faster device response yet does not influence EL efficiencies significantly. Hence, the technique of integrating ionic liquid moieties onto the CTMC directly serves as a useful and promising alternative to improve the turn-on speed of LECs and to realize single-component CTMC LECs compatible with simple driving schemes.

3 White Light-Emitting Electrochemical Cells Based on Cationic Transition Metal Complexes

Although solid-state LECs possess several advantages attractive for lighting applications, rare demonstration of white-emitting solid-state LECs had been reported. The only previous report of solid-state white LECs was based on phase-separated mixture of a polyfluorene derivative and polyethylene oxide (PEO) [10]. However, the fluorescent nature of conjugated polymers would limit the eventual EL efficiency. Recently, CTMCs have also been used in solid-state LECs [11–22, 31, 32, 36, 38, 41, 42, 44–49, 51–60], which show two major advantages over conventional polymer LECs (a) no ion-conducting material (e.g., PEO) is needed since these metal complexes are intrinsically ionic; and (b) higher EL efficiencies could be achieved due to the phosphorescent nature of the transition metal complexes. Inspired by previous works regarding energy transfer between ionic complexes reported by Malliaras [38] and De Cola [60], we had previously demonstrated highly efficient solid-state LEC devices by adopting host–guest cationic metal complexes [49]. Yet to our knowledge, there is no white LECs based on CTMCs ever being reported to date, despite their high potential.

Efficient white light emission may be most easily achieved by mixing two complementary colors, such as blue-green and red emission. Thus, the development of efficient blue-green [21, 22, 44, 60] and red-emitting [11–17, 22, 31, 38, 42, 48, 56] CTMCs is highly desired. In this section, we report the characterization of efficient blue-green and red-emitting cationic iridium complexes and their successful application in white LECs with adopting the effective host–guest strategy [38, 49, 61].

3.1 Photophysical and Electrochemical Properties of Novel Blue-Green and Red-Emitting Cationic Iridium Complexes

Molecular structures of complexes **5**–**8** are shown in Fig. 15. The emission properties of complexes **5**–**8** in solutions (DCM, 10^{-5} M) or in thin films are summarized in Table 5. For reducing the response time of LECs, in this work the ionic liquid

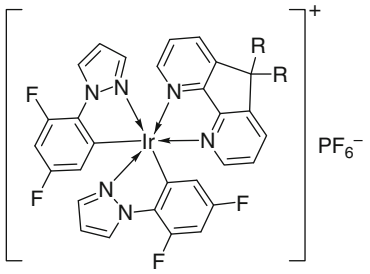

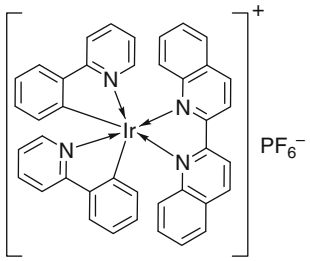

8

5: $[Ir(dfppz)_2(dasb)]^+$ (PF_6^-), R, R = 2, 2′-biphenyl

6: $[Ir(dfppz)_2(bmpdaf)]^+$ (PF_6^-), R, R = 4-CH_3OPh, 4-CH_3OPh

7: $[Ir(dfppz)_2(dedaf)]^+$(PF_6^-), R, R = C_2H_5, C_2H_5

Fig. 15 Molecular structures of complexes **5**–**8**

[BMIM][PF_6] was introduced in the emissive layer to provide additional mobile anions [29, 32, 49]. Thus, emission properties of **5**–**7** films in the presence of [BMIM][PF_6] (19 wt%) were also examined. In general, complexes **5**–**7** show PL peaks at 491–499 nm and rather high PLQYs of 0.46–0.66 in solutions. High PLQYs of these complexes indicate that the rigidity of the daf ligand is beneficial for reducing nonradiative (e.g., vibration) deactivation processes. Among the three blue-green complexes **5**–**7**, **7** exhibits shortest emission wavelengths of 488–491 nm and highest PLQYs of 0.28–0.30 in thin films (neat or dispersed with [BMIM][PF_6], and thus was chosen as the host material for white LEC studies. The absorption and PL spectra of blue-green complex **7** and red-emitting complex **8** in solutions and in neat films (~100 nm) are explicitly shown in Fig. 16. Interestingly, complex **7** with the alkyl substitution on daf exhibits nearly same emission wavelengths in solutions and in solid films. Complex **8** exhibits more saturated red emission (with PL peaks of 656 and 672 nm in solutions and in neat films, respectively) compared with that of $[Ir(ppyz)_2(biq)]PF_6$ [22]. The energy gaps estimated by cyclic voltammetry for complex **8** (2.23 eV, Table 5) and $[Ir(ppyz)_2(biq)]PF_6$ (2.45 eV) [22] are consistent with the photophysical observation. For $[Ir(ppyz)_2(biq)]PF_6$, the HOMO and the LUMO are predominantly localized on the ppz and biq ligand, respectively [22]. The smaller energy gap of complex **8**, which also contains biq, is thus associated with destabilization of HOMO in replacing ppz with ppy.

Cyclic voltammetry was used to probe the electrochemical properties of these complexes. The results are summarized in Table 5. For complexes **5**–**7**, one reversible oxidation potential was detected, which can be attributed to the oxidation that occurred on the Ir center. Interestingly, the electronic nature of ancillary daf ligands plays a subtle role on the oxidation potential. For example, complex **7** containing a more electro-rich dedaf ligand shows a lower oxidation potential (1.20 V) when compared with those of complexes **5** (1.29 V) and **6** (1.28 V), both

Table 5 Summary of physical properties of complexes **5**–**8**

Complex	$\lambda_{max,\ PL}$ (nm), Φ, τ (μs)[a]			$E^{ox}_{1/2}$ (V)[b]	$E^{red}_{1/2}$ (V)[b]	$\Delta E_{1/2}$ (V)
	Solution[c]	Neat film or host–guest film	Film with [BMIM][PF_6][d]			
5	499, 0.46, 0.71	513, 0.20, 0.36	504, 0.22, 0.42	+1.29[e]	−1.70[b]	2.99
6	497, 0.66, 0.85	507, 0.22, 0.51	498, 0.26, 0.56	+1.28[e]	−1.72[f]	3.00
7	491, 0.54, 0.73	491, 0.28, 0.55	488, 0.30, 0.74	+1.20[g]	−1.79[f]	2.99
8	656, 0.20, 0.75	672, 0.09, 0.33	–	+0.86[f]	−1.37[f]	2.23
8 (0.2 wt %) : **7**	–	(493, 606), 0.26, (0.49[h], 1.54[i])	(488, 603), 0.29, (0.54[h], 1.68[i])	–	–	–
8 (0.4 wt %) : **7**	–	(493, 614), 0.27, (0.38[h], 1.52[i])	(488, 612), 0.28, (0.47[h], 1.68[i])	–	–	–

[a]At room temperature
[b]Potential vs. ferrocene/ferrocenium redox couple
[c]Measured in CH_2Cl_2 (10^{-5} M)
[d]Films containing 19 wt% [BMIM][PF_6]
[e]0.1 M tetra-*n*-butylammonium hexafluorophosphate ($TBAPF_6$) in acetonitrile
[f]0.1 M $TBAP_6$ in acetonitrile
[g]0.1 M $TBAPF_6$ in CH_2Cl_2
[h]Measured at 480 nm
[i]Measured at 650 nm
Reproduced with permission from [61]. Copyright 2008, American Chemical Society

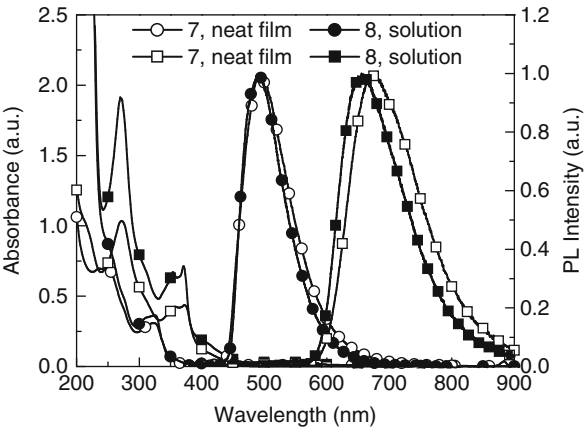

Fig. 16 Absorption (*left*) and PL spectra (*right*) of complexes **7** and **8** in dichloromethane solutions (10^{-5} M) and in neat films. Reproduced with permission from [61]. Copyright 2008, American Chemical Society

containing aryl substitutions on C9 of the diazafluorene ligand. On the contrary, the reduction capability of the diazafluorene ligand is presumably responsible for observed reversible reduction of complexes **5**–**7**. Thus, the Ir-complex coordinated

to an electron-rich dedaf ligand (complex **7**) shows a more negative reduction potential (−1.79 V) when compared with those complexed to the aryl-substituted daf ligand [complexes **5** (−1.70 V) and **6** (−1.72 V)]. These results thus suggest that the energies of frontier orbitals in these complexes can be subtly manipulated by tailoring the electronic properties of the auxiliary daf ligands. For the red complex **8**, one reversible oxidation (0.86 V) and one reversible reduction (−1.37 V) were detected. The electron-rich character of the ppy ligand and the more π-delocalized biq ligand contribute to the higher ease of oxidation and reduction, respectively, thus leading to a small energy gap of complex **8**.

Emission properties of the **7**:**8** host–guest films are also summarized in Table 5. Figure 17 depicts the PL spectra of the host–guest films with different guest **8** concentrations (0.4 and 0.2 wt%) with or without the presence of [BMIM][PF_6] (19 wt%). In general, with the presence of [BMIM][PF_6], both the host and guest exhibit longer excited-state lifetimes and the PLQYs are slightly raised (Table 5), indicating the role of [BMIM][PF_6] in suppressing intermolecular interactions [49]. As shown in Fig. 17, white emission of different blue-green and red compositions can be achieved by adjusting the guest concentration. Raising the guest concentration effectively enhances the host–guest energy transfer, accompanied by shorter lifetimes of the host emission (Table 5). The host–guest film containing 0.4 wt% of **8** (guest) shows white emission having CIE coordinates of (x, y) = (0.34, 0.37), which is rather close to the ideal equal-energy white (x, y) = (0.33, 0.33), and therefore was subjected to further EL studies.

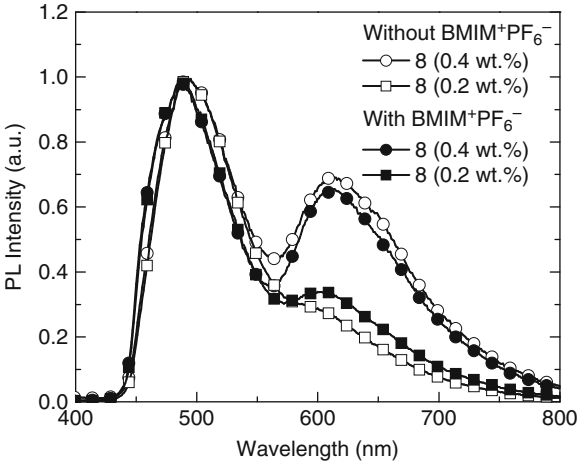

Fig. 17 PL spectra of host–guest films containing different guest concentrations (0.4 and 0.2 wt %) without and with [BMIM][PF_6] (19 wt%). Reproduced with permission from [61]. Copyright 2008, American Chemical Society

3.2 *Electroluminescent Properties of White Light-Emitting Electrochemical Cells Based on Host–Guest Cationic Iridium Complexes*

The LECs have the structure of ITO/emissive layer (100 nm)/Ag (150 nm), where the emissive layer contains host **7** (80.5 wt%), guest **8** (0.4 wt%), and [BMIM][PF_6] (19.1 wt%). Their EL properties are summarized in Table 6. The EL spectra of the white LECs under various biases, along with the PL spectra for comparison, are shown in Fig. 18a. It is noted that the peak wavelength of the blue component in EL spectra is 488 nm, which is one of the shortest EL wavelengths reported to date for LECs based on CTMCs. Compared with PL, the relative intensity of the red emission with respect to the blue emission is larger in EL and increases as the bias decreases. Furthermore, the maximum current density of the host–guest device (with 0.4 wt%

Table 6 Summary of white LEC device characteristics

Bias (V)	CIE (x, y)[a]	CRI[a]	t_{max}[b] (min)	L_{max}[c] (cd m^{-2})	$\eta_{ext,\,max}$, $\eta_{L,\,max}$, $\eta_{p,\,max}$[d] (%, cd A^{-1}, lm W^{-1})	$t_{1/2}$[e] (h)
2.9	(0.45, 0.40)	81	240	2.5	4.0, 7.2, 7.8	8.9
3.1	(0.37, 0.39)	80	60	18	3.4, 6.1, 6.2	1.3
3.3	(0.35, 0.39)	80	30	43	3.3, 5.8, 5.5	0.4

[a]Evaluated from the EL spectra
[b]Time required to reach the maximal brightness
[c]Maximal brightness achieved at a constant bias voltage
[d]Maximal external quantum efficiency, current and power efficiencies achieved at a constant bias voltage
[e]The time for the brightness of the device to decay from the maximum to half of the maximum under a constant bias voltage
Reproduced with permission from [61]. Copyright 2008, American Chemical Society

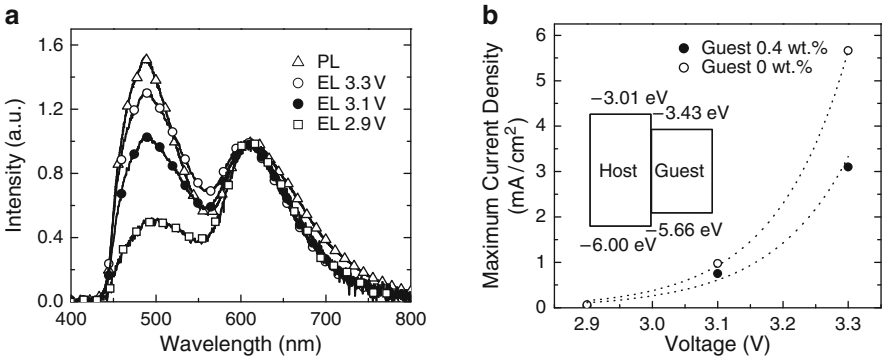

Fig. 18 (**a**) The bias-dependent EL spectra of the white LECs compared with the PL spectrum. (**b**) Maximum current density vs. voltage characteristics for the host–guest (0.4 wt% doping concentration) and the host-only LECs. *Inset*: the energy level diagram of the host and guest molecules. Reproduced with permission from [61]. Copyright 2008, American Chemical Society

guest) is lower than that of the host-only device under same bias conditions (Fig. 18b). These results could be understood by energy level alignments of the host and guest (inset of Fig. 18b). At lower biases, such energy level alignments favor carrier injection and trapping on the smaller-gap guest, resulting in direct carrier recombination/exciton formation on the guest (rather than host– guest energy transfer). Therefore, larger fractions of guest emission are observed at lower biases. Nevertheless, white emission with CIE coordinates of (0.35, 0.39) could be achieved at higher biases and brightness. Also, the present white LECs exhibit a rather high color rendering index (CRI) (up to 80), which is an important characteristic for solid-state lighting.

Figure 19a shows the time-dependent brightness and current density under constant biases of 2.9–3.3 V for the white LEC. After the bias was applied, the current first rose and then stayed rather constant. On the contrary, the brightness first increased with the current and reached the maxima of 2.5 cd m^{-2}, 18 cd m^{-2}, and 43 cd m^{-2} under biases of 2.9 V, 3.1 V, and 3.3 V, respectively. The brightness then dropped with time with a rate depending on the bias voltage (or current). Corresponding time-dependent EQEs and power efficiencies of the same device are shown in Fig. 19b. When a forward bias was just applied, the EQE was rather low due to poor carrier injection. During the formation of the doped regions near electrodes, the capability of carrier injection was improved and the EQE thus rose rapidly. The peak EQEs, current and power efficiencies at 2.9 V, 3.1 V, and 3.3 V are (4.0%, 7.2 cd A^{-1}, 7.8 lm W^{-1}), (3.4%, 6.1 cd A^{-1}, 6.2 lm W^{-1}), and (3.3%, 5.8 cd A^{-1}, 5.5 lm W^{-1}), respectively.

Peak brightness and turn-on time (the time required to reach the maximal brightness) as a function of bias voltage for white LECs are shown in Fig. 20a. An electrochemical junction between p- and n-type doped layers of LECs is formed during device operation. As revealed in previous studies [31], as bias voltage increases, the junction width decreases due to extension of doped layers, consequently leading to higher current density (Fig. 19a) and higher brightness (Fig. 20a). The higher electric field in the device also accelerates redistribution of mobile ions,

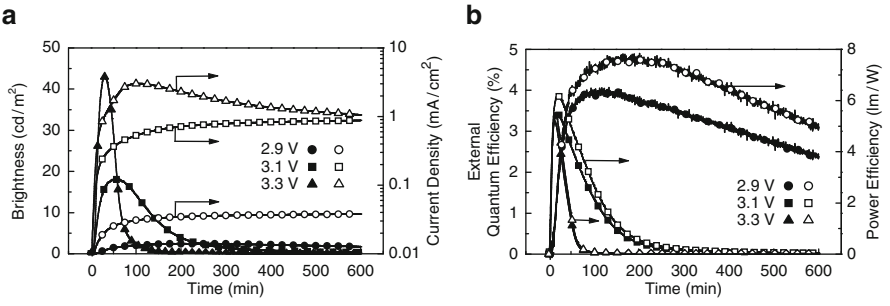

Fig. 19 (**a**) Brightness (*solid symbols*) and current density (*open symbols*) and (**b**) external quantum efficiency (*solid symbols*) and power efficiency (*open symbols*) as a function of time under a constant bias voltage of 2.9–3.3 V for the white LEC. Reproduced with permission from [61]. Copyright 2008, American Chemical Society

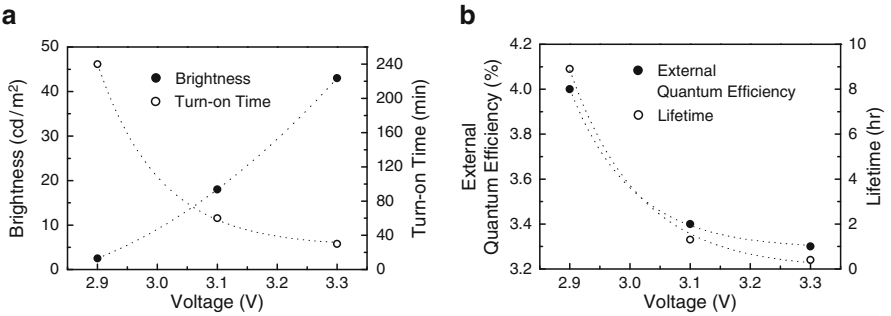

Fig. 20 (**a**) Peak brightness (*solid symbols*) and turn-on time (*open symbols*) and (**b**) peak external quantum efficiency (*solid symbols*) and lifetime (*open symbols*) as a function of bias voltage for the white LECs. Reproduced with permission from [61], American Chemical Society

which facilitates formation of ohmic contacts with the electrodes. Thus, operation of LECs under higher bias voltages speeds up the device response (Fig. 20a). However, higher brightness and faster response are obtained at the expense of device stability. As shown in Fig. 20b, peak EQE and device lifetime (the time for the brightness of the device decaying from the maximum to half of the maximum under a constant bias voltage) of the white LECs deteriorate under higher bias voltages. It may be associated with the fact that the higher electric field or current density accelerates degradation (multiple oxidation and subsequent decomposition) [32] of the emissive CTMCs. Previous studies showed that addition of materials altering the electronic properties of the emissive layer of LECs also influence the device lifetimes [14, 56]. Blending an inert polymer [14] in the emissive layer of LECs improves device lifetimes, while addition of an electrolyte [56] shortens device lifetimes. Blending of an inert polymer reduces the electronic conductivity of the emissive layer and thus lowers the current density. On the contrary, additional mobile ions provided by the electrolyte increase the doping level of the doped region, resulting in higher current density due to increased electronic conductivity. These results also imply that higher current leads to shorter device lifetimes. Recently, two reports [52, 53] have revealed that electrical driving of LECs based on CTMCs induces oxo-bridged dimers, which effectively quench EL. However, detailed degradation mechanisms of the LECs based on CTMCs remain unclear and further studies are still needed to achieve practical device lifetimes.

4 Outlook

Solid-state CTMC-based LECs exhibit advantages of simple fabrication processes, low-voltage operation, and high power efficiency, which thus may be competitive for lighting applications. However, improvements will be required in our prototype

white CTMC-based LECs for practical applications. For device efficiencies, measured device efficiency did not reach the upper limit (~6%) estimated from the PLQY of the emissive layer (~30%) and ~20% light out-coupling efficiency from a typical layered light-emitting device structure. It may be associated with exciton quenching by one of the electrodes if there is discrepancy in electron and hole transport, rendering the recombination zone closer to one of the electrodes. To further improve the device efficiency, further tailoring of molecular structures to achieve more balanced electron and hole transport is required. Improving device lifetimes will also be essential for lighting applications. Introducing functional groups with resistance against quencher formation and/or electrochemical degradation in CTMCs will facilitate realization of long-lifetime white LECs for lighting applications.

References

1. Kido J, Hongawa K, Okuyama K et al (1994) Appl Phys Lett 64:815
2. Tokito S, Iijima T, Tsuzuki T et al (2003) Appl Phys Lett 83:2459
3. D'Andrade BW, Forrest SR (2004) Adv Mater 16:1585
4. Gong X, Wang S, Moses D et al (2005) Adv Mater 17:2053
5. Huang J, Li G, Wu E et al (2006) Adv Mater 18:114
6. Tang CW, VanSlyke SA (1987) Appl Phys Lett 51:913
7. Burroughes JH, Bradley DDC, Brown AR et al (1990) Nature 347:539
8. Pei Q, Yu G, Zhang C et al (1995) Science 269:1086
9. Pei Q, Yang Y, Yu G et al (1996) J Am Chem Soc 118:3922
10. Yang Y, Pei Q (1997) J Appl Phys 81:3294
11. Lee JK, Yoo DS, Handy ES et al (1996) Appl Phys Lett 69:1686
12. Handy ES, Pal AJ, Rubner MF (1999) J Am Chem Soc 121:3525
13. Gao FG, Bard AJ (2000) J Am Chem Soc 122:7426
14. Rudmann H, Rubner MF (2001) J Appl Phys 90:4338
15. Liu CY, Bard AJ (2002) J Am Chem Soc 124:4190
16. Rudmann H, Shimada S, Rubner MF (2002) J Am Chem Soc 124:4918
17. Liu CY, Bard AJ (2005) Appl Phys Lett 87:061110
18. Slinker JD, Gorodetsky AA, Lowry MS et al (2004) J Am Chem Soc 126:2763
19. Lowry MS, Hudson WR, Pascal RA et al (2004) J Am Chem Soc 126:14129
20. Slinker JD, Koh CY, Malliaras GG et al (2005) Appl Phys Lett 86:173506
21. Lowry MS, Goldsmith JI, Slinker JD et al (2005) Chem Mater 17:5712
22. Tamayo AB, Garon S, Sajoto T et al (2005) Inorg Chem 44:8723
23. Wu CC, Lin YT, Chiang HH et al (2002) Appl Phys Lett 81:577
24. Wong KT, Chien YY, Chen RT et al (2002) J Am Chem Soc 124:11576
25. Wu CC, Liu TL, Hung WY et al (2003) J Am Chem Soc 125:3710
26. Wu CC, Lin YT, Wong KT et al (2004) Adv Mater 16:61
27. Chao TC, Lin YT, Yang CY et al (2005) Adv Mater 17:992
28. Wong KT, Chen RT, Fang FC et al (2005) Org Lett 7:1979
29. Su HC, Fang FC, Hwu TY et al (2007) Adv Funct Mater 17:1019
30. Kawamura Y, Goushi K, Brooks J et al (2005) Appl Phys Lett 86:071104
31. Rudmann H, Shimada S, Rubner MF (2003) J Appl Phys 94:115
32. Parker ST, Slinker JD, Lowry MS et al (2005) Chem Mater 17:3187
33. Yang C, Sun Q, Qiao J et al (2003) J Phys Chem B 107:12981

34. Edman L, Pauchard M, Moses D et al (2004) J Appl Phys 95:4357
35. Wenzl FP, Pachler P, Suess C et al (2004) Adv Funct Mater 14:441
36. Kalyuzhny G, Buda M, McNeill J et al (2003) J Am Chem Soc 125:6272
37. Tang CW, VanSlyke SA, Chen CH (1989) Appl Phys Lett 65:3610
38. Hosseini AR, Koh CY, Slinker JD et al (2005) Chem Mater 17:6114
39. Chen FC, Yang Y, Pei Q (2002) Appl Phys Lett 81:4278
40. Sinanoğlu O (1965) Modern quantum chemistry. Academic, New York
41. Ng WY, Gong X, Chan WK (1999) Chem Mater 11:1165
42. Bolink HJ, Cappelli L, Coronado E et al (2005) Inorg Chem 44:5966
43. Sauvage JP, Collin JP, Chambron JC et al (1994) Chem Rev 94:993
44. Nazeeruddin MK, Wegh RT, Zhou Z et al (2006) Inorg Chem 45:9245
45. Bolink HJ, Cappelli L, Coronado E et al (2006) Chem Mater 18:2778
46. Maness KM, Terrill RH, Meyer TJ et al (1996) J Am Chem Soc 118:10609
47. Maness KM, Masui H, Wightman RM et al (1997) J Am Chem Soc 119:3987
48. Bernhard S, Barron JA, Houston PL et al (2002) J Am Chem Soc 124:13624
49. Su HC, Wu CC, Fang FC et al (2006) Appl Phys Lett 89:261118
50. Ohsawa Y, Sprouse S, King KA et al (1987) J Phys Chem 91:1047
51. Rudmann H, Shimada S, Rubner MF et al (2002) J Appl Phys 92:1576
52. Soltzberg LJ, Slinker JD, Flores-Torres S et al (2006) J Am Chem Soc 128:7761
53. Slinker JD, Kim JS, Flores-Torres S et al (2007) J Mater Chem 17:76
54. Bolink HJ, Cappelli L, Coronado E et al (2006) J Am Chem Soc 128:14786
55. Lee KW, Slinker J, Gorodetsky AA et al (2003) Phys Chem Chem Phys 5:2706
56. Lyons CH, Abbas ED, Lee JK et al (1998) J Am Chem Soc 120:12100
57. Leprêtre JC, Deronzier A, Stephan O (2002) Synth Met 131:175
58. Zysman-Colman E, Slinker JD, Parker JB et al (2008) Chem Mater 20:388
59. Su HC, Chen HF, Wu CC et al (2008) Chem Asian J 3:1922
60. Coppo P, Duati M, Kozhevnikov VN et al (2005) Angew Chem Int Ed 44:1806
61. Su HC, Chen HF, Fang FC et al (2008) J Am Chem Soc 130:3413